ICEF 2022-91028

Development of a Synthetic Surrogate for F-24 from Blends of Iso-Paraffinic Kerosene (IPK) and Fischer-Tropsch Synthetic Kerosene (S8) in a Constant Volume Combustion Chamber (CVCC)

Valentin Soloiu¹, Lily Parker¹, Richard Smith III¹, Amanda Weaver¹, Austin Brant¹, Aidan Rowell¹, Marcel Ilie¹

¹Combustion Laboratory, Georgia Southern University, Statesboro, GA, USA

Abstract

Investigations were conducted using mass blends of Iso-Paraffinic Kerosene (IPK) and Fischer-Tropsch Synthetic Kerosene (S8) to produce a synthetic surrogate for aerospace F-24. Due to the fossil fuel origin of F-24, the introduction of a synthetic surrogate would create a sustainable aviation fuel (SAF) with sources obtained from within the United States. An analysis of ignition delay (ID), combustion delay (CD), derived cetane number (DCN), negative temperature coefficient (NTC) region, Low-Temperature Heat Release region (LTHR) and High-Temperature Heat Release (HTHR) was conducted using a PAC CID 510 Constant Volume Combustion Chamber (CVCC). The fuels examined in this study are neat IPK, neat S8, neat F-24, and by mass percentages, as follows: 75IPK 25S8, 52IPK 48S8, 51IPK 49S8, 50IPK 50S8 and 25IPK 75S8.

The DCN values determined for IPK, S8, and F-24 were 26.92, 59.56 and 44.35 respectively. The influence of IPK present in the blends increases CD, thus reducing the DCN significantly. The fuel blend of 50IPK 50S8 was observed to be the closest match to F-24 when comparing DCN, ID and CD.

The surrogate blends were determined to have a lower magnitude of peak pressure ringing compared to that of the neat S8 and F-24, this is due to the extended NTC region caused by the IPK present in the blend. During further refinement of the surrogate blend, the Apparent Heat Release Rate (AHRR) curve for the 51IPK 49S8 fuel blend was found to have the closest match to the AHRR of F24. The surrogate blend 50IPK 50S8 was shown to have the smallest percent difference and best match during the LTHR stage, compared to F-24, while 52IPK 48S8 had the smallest percent difference for the energy released during LTHR. The ID and CD of the 25/75% blends were too dissimilar from the F-24 target to be considered as a surrogate.

A Noise Vibration Harshness (NVH) analysis was also conducted during the combustion of the three neat fuels in the CVCC. This analysis was conducted to relate the ID, CD, HTHR and ringing to the vibrations that occur during combustion. Neat S8 was observed to have the most vibrations occurring during the combustion process. Additionally, the HTHR was observed

to have a distinct pattern for the three neat fuels and the combustion of these fuels was quieter overall.

Nomenclature

ATIDD

AHRR	Apparent Heat Release Rate
CD	combustion delay
CVCC	Constant Volume Combustion Chamber
DCN	Derived Cetane Number
DTA	Differential Thermal Analysis
Dv(x)	Largest Droplet Size Observed in x% of spray
	by volume
EOC	End of Combustion
F-T	Fischer-Tropsch
HTHR	High-Temperature Heat Release
ID	Ignition Delay
IPK	Iso-Paraffinic Kerosene
LHV	Lower Heating Value
LTC	Low-Temperature Combustion
LTHR	Low-Temperature Heat Release
SAF	Sustainable Aviation Fuels
SMD	Sauter Mean Diameter
SOC	Start of Combustion
SOI	Start of Injection
S8	Fischer-Tropsch Synthetic Kerosene
TA(x)	Temperature at which X% of fuel is Vaporized
TGA	Thermogravimetric Analysis
NTC	Negative Temperature Coefficient
NVH	Noise Vibration Harshness

Introduction

Society today is dependent on fossil fuels as a primary source of energy, making the availability of them a growing concern. This, along with harmful emissions produced during combustion, necessitates the development of sustainable fuel replacements.

Neat F-24 is a high-altitude fuel with military applications derived from the parent fuel Jet-A with additives to minimize corrosion, static charge and increase lubricity [1]. Iso-Paraffinic Kerosene (IPK) and Fischer-Tropsch Synthetic Kerosene (S8) are both Fischer-Tropsch Sustainable Aviation Fuels (SAF). The combustion of IPK has been known to have reduced gaseous emissions while maintaining high thermal efficiency [2-8]. The aviation industry has committed to reducing emissions, making SAF options an important step to becoming carbon neutral and reducing greenhouse gases [9-10]. As SAF options provide a more diverse fuel supply, fluctuations in fuel prices can be reduced while also providing regional economic benefits [11-12].

The Fischer-Tropsch process (F-T) is a method by which synthetic hydrocarbon fuels are derived from sources such as biomass, coal, and natural gas. This is usually done through the conversion of syngas [13-14]. The chemical equations for the alkene and alkane formation of the F-T hydrocarbon synthesis are summarized in Equations 1 and 2.

$$2nH_2 + nCO \rightarrow C_nH_{2n} + nH_2O$$
 Eq. 1

$$(2n+1)H_2 + nCO \rightarrow C_nH_{(2n+2)} + nH_2O$$
 Eq. 2

The F-T process is highly advantageous as it is less complex, which provides greater economic feasibility and produces more environmentally friendly fuels than traditional petroleum-based fuels and processes [15-19]. Due to current limitations in infrastructure, F-T fuels cannot be used as a drop-in replacement for current engines in the United States, thus research is required to develop surrogate blends.

A Constant Volume Combustion Chamber (CVCC) was used to determine the combustion properties, such as autoignition, rates of temperature rise, pressure rise, and the apparent heat release of fuels in a controlled environment [19, 20]. Alhikami et al [21] studied the spray ignition characteristics of JP-5, Jet-A, and HRJ in a CVCC, varying temperature and pressure. Fuel reactivity was found to increase with chamber pressure and ignition delays shortened exponentially with increased chamber pressure. The NTC region was also a factor of study as it is important to the study of LTHR.

Materials and Methods

Spray Atomization and Droplets' Distribution Analysis using Mie Scattering He-Ne Laser

Mie scattering theory was utilized in a He-Ne Malvern Spraytec laser diffraction particle analyzer to determine the Sauter Mean Diameter (SMD) and spray droplet size distribution of the researched fuels after atomization. The research apparatus, shown in Figure 1, is composed of a pintle type Bosch fuel injector pressurized at 180 Bar that is perpendicularly positioned 100mm away from the laser beam. The sensor array is composed of 36 silicon diode detectors that measure droplets from $0.1 \mu m$ to $900 \mu m$ at a rate of 10 kHz. For this study, 28 of the sensors (8

to 36) were selected. Measurements occurred 1ms after the start of injection for a duration of 5ms. All testing was conducted in ambient air at standard temperature and pressure.

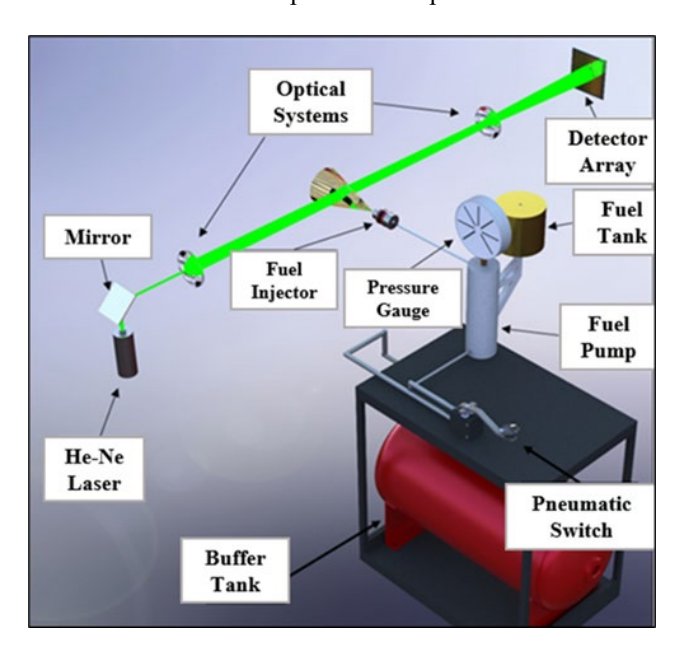


Figure 1. Mie Scattering He-Ne Malvern Spraytec Laser

Thermogravimetric Analysis (TGA) and Differential Thermal Analysis

A Thermogravimetric Analysis (TGA) and Differential Thermal Analysis (DTA) were conducted to determine the volatility and low-temperature energy release of the neat fuels. Samples of the fuels are placed in a controlled chamber that heats the sample from 20°C to 600°C at a rate of 20°C/min. The chamber is constantly purged with air at a flow rate of 15mL/min. The change in mass of the fuel is measured as a percentage of the initial mass.

PAC CID 510 Constant Volumes Combustion Chamber

The PAC CID 510 Constant Volume Combustion Chamber (CVCC) was utilized to determine the Ignition Delay (ID) and Combustion Delay (CD) which was then utilized to calculate the Derived Cetane Number (DCN) of the researched fuels. The internal components of the CVCC are shown in Figure 2 with values corresponding to Table 1.

Table 1. Internal Components of PAC CID 510 CVCC

Component 1	High-pressure Common Rail Fuel	
	Injection System	
Component 2	6 Orifice Bosch Fuel Injector	
Component 3	Combustion Chamber	
Component 4	In-Chamber Piezoelectric Pressure Sensor	
Component 5	Injection Pressure Sensor	

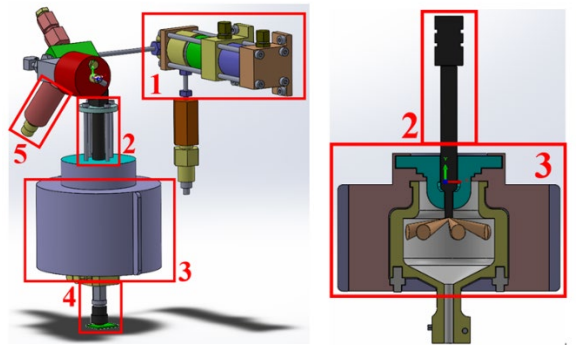


Figure 2. PAC CID 510 Internal Components (CAD model)

Approximately 60mg of fuel is injected into the chamber per cycle before analysis is conducted. The CVCC performs five conditioning cycles to prime the chamber and flush out old fuel. Following the conditioning cycles, 15 cycles of injection, combustion and exhaust are completed using the ASTM standard D7668-14a testing parameters shown in Table 2. Due to the differences in viscosity of each fuel, the amount of mass injected into the chamber can differ by up to 2%.

Table 2. Standard Testing Parameters

Wall	Fuel Inj.	Coolant	Inj. Pulse	Chamber
Temp.	Pressure	Temperature	Width	Pressure
595.5°C	1000 Bar	50 °C	2.5 ms	20 Bar

Discussion and Results: Thermophysical Properties of the Researched fuels

The viscosity of the neat fuels was analyzed because of the influence this property has on spray distribution. At 40°C neat F-24 was observed to have the highest viscosity at 1.37cP, while IPK had the lowest at 1.04cP. Fuels with higher viscosities have a lower surface area and that leads to more incomplete combustion [22]. The lower heating value of the neat fuels was analyzed to determine the heat of combustion, as a higher LHV is correlated with a higher hydrocarbon ratio in the fuel [23, 24]. The LHV ranged from 41.85 to 44.25 MJ/kg for all the researched fuels. The results of the thermophysical analysis of the tested fuels in a CVCC and can be seen in Table 3.

Table 3.	Thermophysi	cal Properties

Table 5. Thermophysical Troperties						
Fuels	100	100	75IPK	50IPK	25IPK	100
	F-24	IPK	25S8	50S8	75S8	S8
POSF no.	13664	7629	ı	•	ı	5109
LHV-	41.85	44.25	-	-	-	42.04
MJ/kg						
DCN*	44.35	26.92	37.14	44.56	51.48	59.56
Avg.ID	3.90	4.62	4.01	3.45	3.10	2.81
(ms)						
Avg.CD	5.59	15.45	7.55	5.52	4.62	4.04
(ms)						
Visc. @	1.37	1.04	-	-	-	1.28
40°C (cP)						

^{*} DCN with PAC CID 501 and ASTM D7668-14a.

Sauter Mean Diameter and Spray Development

The average SMD for the neat fuels is shown in Table 4 where F-24 was observed to have the largest average SMD of the neat fuels. The relationship between the spray volume frequency, droplet size and the SMD over time is shown in Figure 3.

Table 4. Sauter Mean Diameter of Researched Fuels

Researched Fuels	SMD [µm]
100 F-24	18.70
100 IPK	12.50
100 S8	18.83

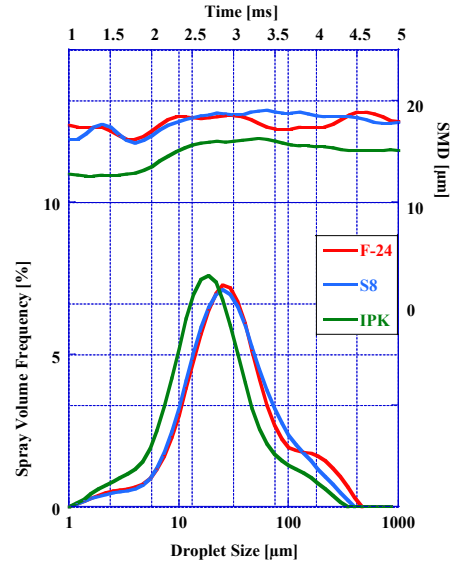


Figure 3. Spray Development of the Neat Fuels

The particle size by volume is shown in Table 5 where Dv(10), Dv(50) and Dv(90) denote 10%, 50% and 90% of the spray droplets that are less than or equal to the diameter. Neat S8 has the largest Dv(10) value, while F-24 is observed to have the largest values for Dv(50) and Dv(90). These larger values for Dv(50) and Dv(90) correlate to F-24 spray being composed of larger droplet sizes. These large droplet sizes are due to the high viscosity of the fuel and may lead to an increase of unburned hydrocarbons in the combustion chamber.

Table 5. Particle Size by Volume

Researched Fuels	Dv (10)	Dv (50)	Dv (90)
	[µm]	[µm]	[µm]
100 F-24	9.96	30.45	133.33
100 IPK	8.27	22.96	103.34
100 S8	10.06	30.03	108.87

Low-Temperature Oxidation and Differential Thermal Analysis

As shown in the TGA curve in Figure 4, neat IPK vaporizes at lower temperatures than S8 and F-24. In Table 6 the temperature of the fuels is observed when 10%, 50%, and 90% of the sample mass is vaporized and is denoted by TA(10),

TA(50) and TA(90). Neat IPK was found to have the lowest values for TA(10), TA(50) and TA(90), at 72°C, 108°C and 131°C respectively. Neat F-24 has the slowest vaporization with a TA(90) approximately 31% higher than that of IPK. The TGA curve of IPK occurs at lower temperatures which indicates the presence of lighter hydrocarbons present in the fuel and higher volatility. This high volatility leads to an earlier and better airfuel mixture in the combustion chamber and a reduction in unburned hydrocarbons.

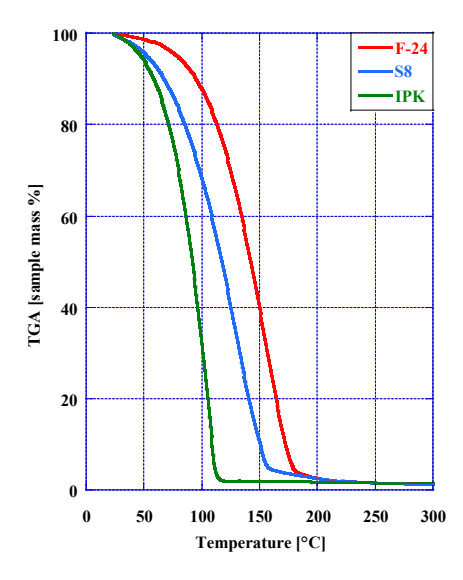


Figure 4. Thermogravimetric Analysis of Neat Fuels

Table 6. Thermogravimetric Analysis (TGA)

Researched Fuels	TA (10)	TA (50)	TA (90)
100 F-24	95°C	142°C	172°C
100 IPK	72°C	108°C	131°C
100 S8	78°C	126°C	162°C

The DTA of the neat fuels, shown in Figure 5, is used to determine the endothermic and exothermic reactions of the fuel as the samples vaporize in a controlled environment. In Figure 5, the negative slope of the curve indicates an endothermic reaction, while the positive slope indicates an exothermic reaction. Furthermore, the slope of the DTA curve indicates the rate at which energy is absorbed and released. As the temperature within the chamber is increased the fuel absorbs heat to a point in which it starts oxidizing, approximately at TA(90), marking the point where the chemical bonds within the fuel break down and energy is released [25]. Neat IPK is shown to absorb and release energy faster than S8 and F-24, with a lower peak value.

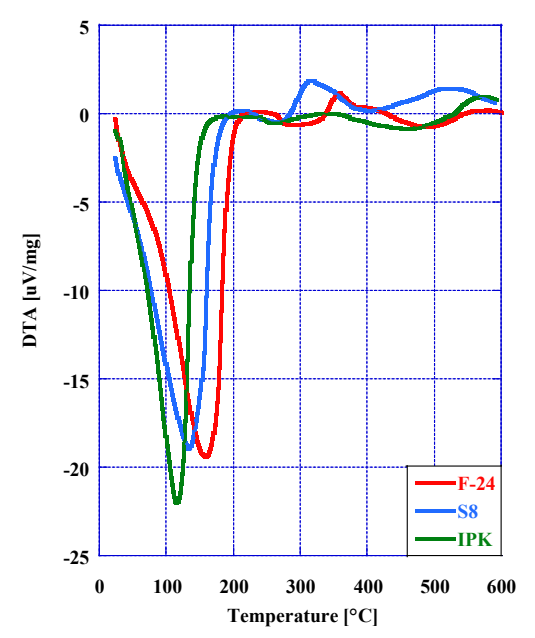


Figure 5. Differential Thermal Analysis

ID, CD, and DCN

The average ID and CD from the 15 cycles are used to calculate the DCN, using Equation 3. In this study, the ID is defined as the duration from the start of injection (0 milliseconds) to the start of combustion. While CD is defined at the duration from the start of injection to the mid-point of the pressure curve, based on [25] and shown in Figure 6.

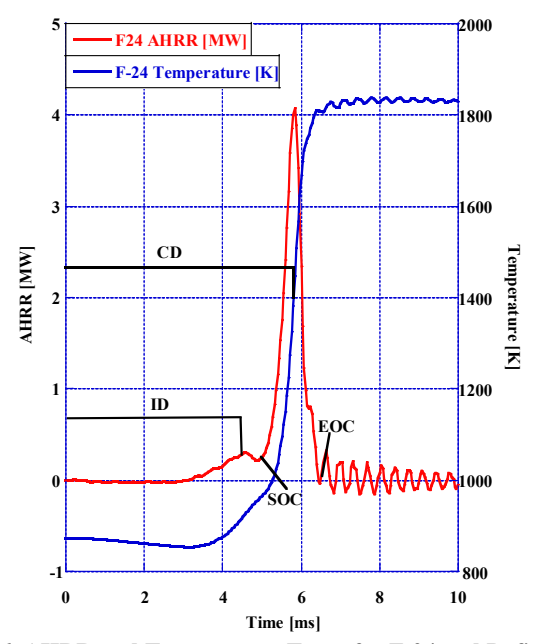


Figure 6. AHRR and Temperature Trace for F-24 and Defined Regions of ID, CD, SOC, and EOC

$$DCN = 13.028 + \left(-\frac{5.3378}{ID}\right) + \left(\frac{300.18}{CD}\right) + \left(-\frac{12567.90}{CD^2}\right) + \left(\frac{3415.32}{CD^3}\right)$$

The average ID, CD and DCN for the researched fuels can be found in Table 7. Neat IPK was observed to have the lowest DCN at 26.92, followed by F-24 at 44.35 and S8 at 59.56. The lower DCN of IPK can be attributed to the high values for ID and CD at 4.62ms and 15.45ms. The DCN of the fuel blends decreases with the addition of IPK in the blends. The fuel blend 75IPK 25S8 had a DCN of 37.14, 50IPK 50S8 had a DCN of 44.56 and 25IPK 75S8 had a DCN of 51.48. The ID and CD of the blends were also observed to increase as IPK increased. The ID of 75IPK 25S8 was 4.01ms, 50IPK 50S8 had an ID of 3.45ms and 25IPK 75S8 had an ID of 3.10ms. The CD of 75IPK 25S8 was 7.55ms, 50IPK 50S8 had a CD of 5.52ms and 25IPK 75S8 had a CD of 4.62ms.

Table 7. ID, CD, and DCN of the Researched Fuels

Researched Fuels	100 F-24	100 IPK	100 S8	75IPK 25S8	50IPK 50S8	25IPK 75S8
DCN*	44.35	26.92	59.56	37.14	44.56	51.48
Avg.ID (ms)	3.90	4.62	2.81	4.01	3.45	3.10
Avg.CD (ms)	5.59	15.45	4.04	7.55	5.52	4.62

The relationship that ID and CD have on the DCN of the fuels is observed in Figure 7. The influence of CD on DCN increases exponentially as the presence of IPK increases in the fuel blends. In contrast, ID increases linearly as IPK% increases. This causes the DCN of the fuels to drastically decrease.

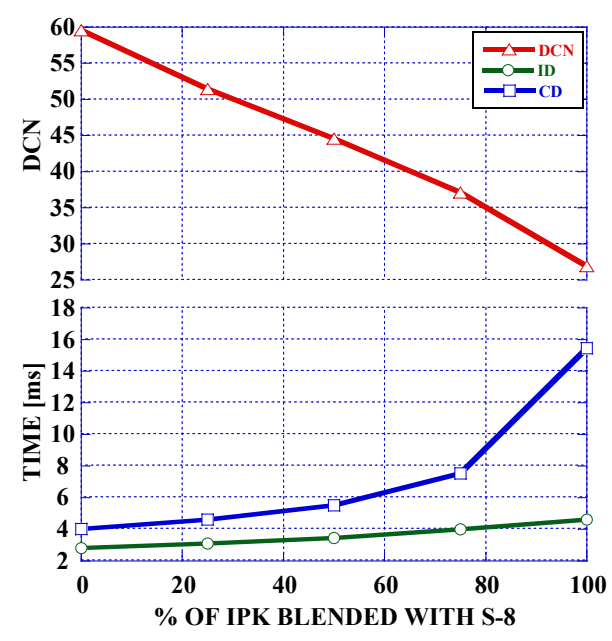


Figure 7. Derived Cetane Number, Ignition Delay, and Combustion Delay of the Researched Fuels

Combustion Pressure and Mass Fraction Burned

The combustion pressure of the researched fuels was measured using a piezoelectric pressure sensor across 15 combustion cycles. This data is averaged and used to determine the AHRR and temperature of the fuels. The pressure curve for the researched fuels can be observed in Figures 8 and 9. The slope of the pressure trace curve is an indication of stability during combustion and oscillations observed during the peak pressure represent ringing which is a result of the dynamic change of pressure gradient in the combustion chamber.

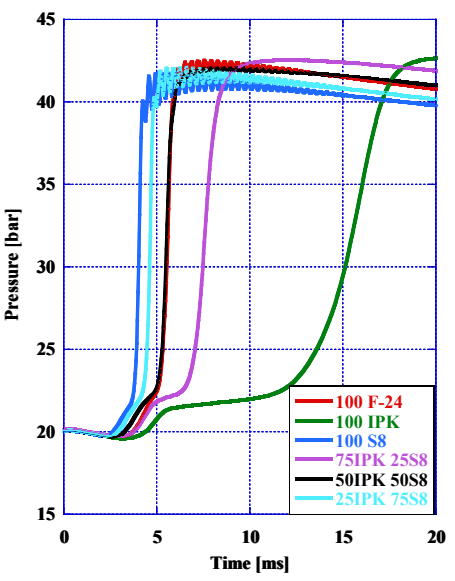


Figure 8. Pressure Curves of the Researched Fuels

Figure 9 shows the combustion pressure of the surrogate fuels under consideration. The fuel blends of 52IPK 48S8, 51IPK 49S8, and 50IPK 50S8 were seen to nearly overlap with the pressure curve for F-24 while having a lower magnitude of ringing at peak pressure, as seen in Figure 10. This lower ringing intensity during peak pressure correlates to more stable combustion for the surrogate fuels.

The peak pressure for all researched fuels can be found in Table 8. Neat IPK was observed to have the largest peak pressure at 42.66 bar, while 25IPK 75S8 had the lowest at 41.11 bar.

Table 8. Peak Pressures of Researched Fuels

Researched Fuels	Peak Pressure (bar)
100 F-24	42.52
100 IPK	42.66
100 S8	41.77
75IPK 25S8	42.54
52IPK 48S8	42.14
51IPK 49S8	42.13
50IPK 50S8	42.09
25IPK 75S8	41.11

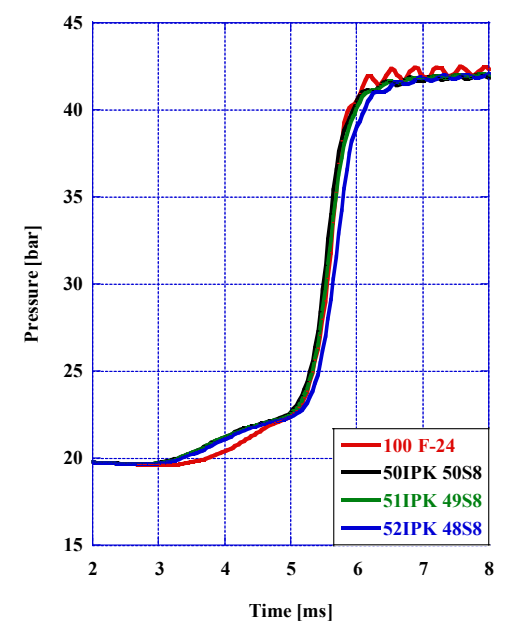


Figure 9. Pressure Curves of the Surrogate Fuels

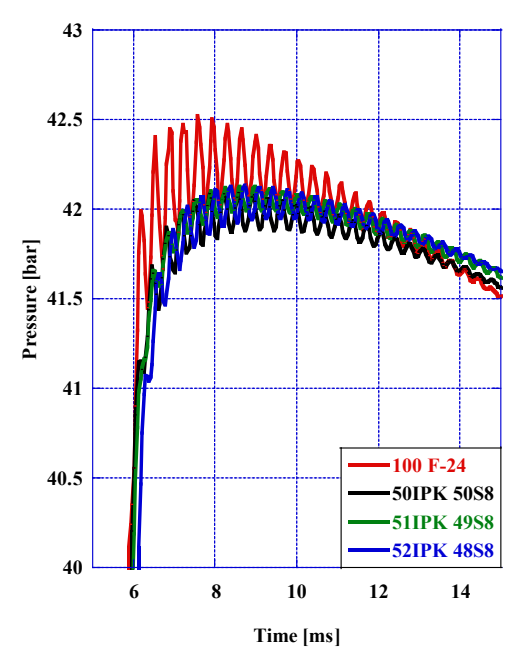


Figure 10. Peak Pressure detail of the Surrogate Fuels

AHRR, NTC Region, and LTHR Analysis

The AHRR is defined as the amount of energy required to raise the temperature of the combustion chamber. To conduct AHRR analysis, the conditions within the CVCC are considered adiabatic and 100% combustion efficiency is assumed, allowing for a closed system analysis governed by Equation 4. The global specific heat ratio is assumed to be constant; the injection was considered to be homogeneous, and the step count is constant throughout the combustion cycle at 0.04ms.

$$\frac{dQ}{dt} = \frac{1}{\gamma - 1} V \frac{dP}{dt}$$
 Eq. 4

The AHRR curve for the researched fuels is shown in Figure 11. The peak AHRR for the surrogate fuels is seen in Figure 12, where 50IPK 50S8 is observed to have the closest peak AHRR to F-24, while 51IPK 49S8 is observed to have the closest AHRR trend to F-24. Neat S8 and 25IPK 75S8 were observed to produce strong ringing after HTHR phase of combustion, as seen in Figure 11, after 5ms mark.

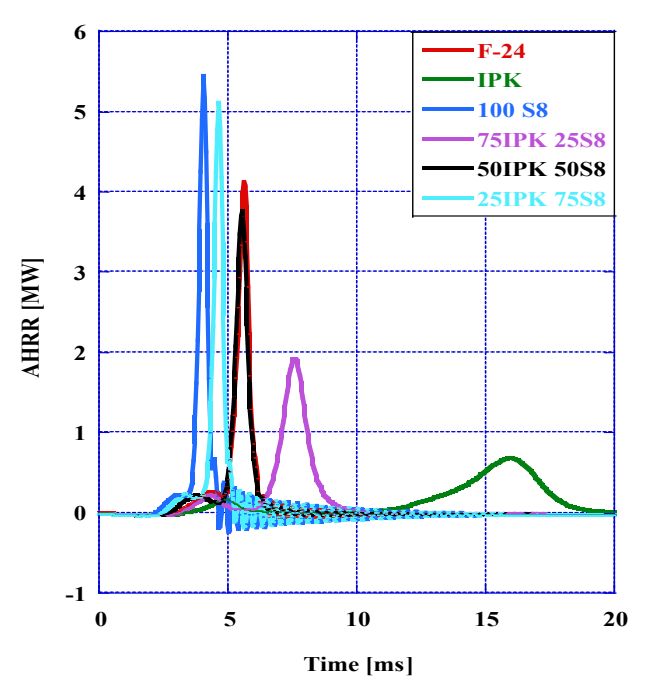


Figure 11. AHRR of the Researched Fuels

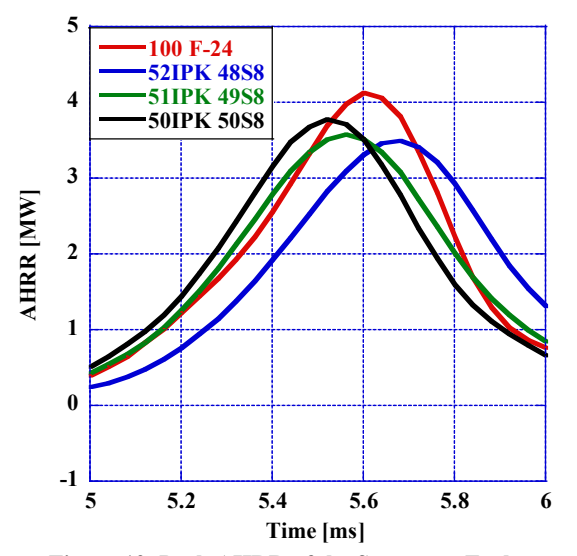


Figure 12. Peak AHRR of the Surrogate Fuels

The Low-Temperature Heat Release (LTHR) region is a period during which the fuels undergo periods of slow oxidation and cool flame formation. During the formation of cool flames there are periods of ignition and quenching of about 0.5ms, best seen on F-24 in Figure 13, that vary with the hydrocarbon structure of each fuel. Hydrocarbon structure influences ignition timing, burn rate, burning limits, knock and emissions [25, 26, 27].

The Low-Temperature Heat Release (LTHR) region, Negative Temperature Coefficient, and the cool flame formation region for this study are defined in Figure 13 and the LTHR regions for the surrogate fuels are shown in Figure 14.

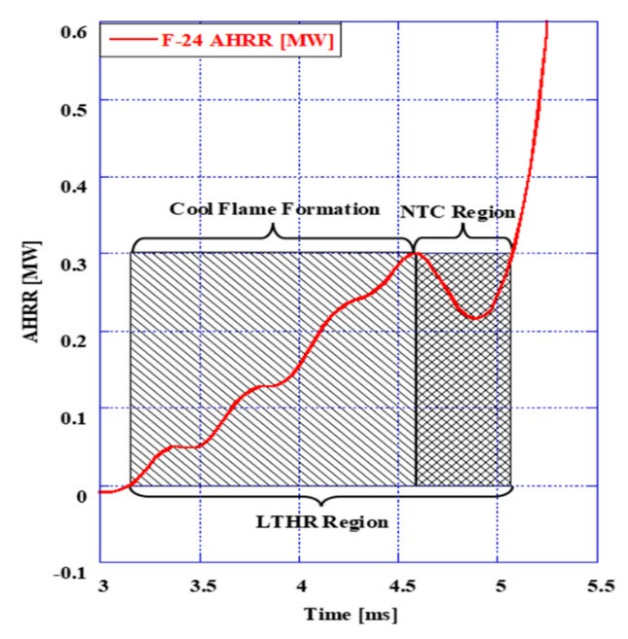


Figure 13. LTHR, Cool Flame Formation, and NTC of F-24

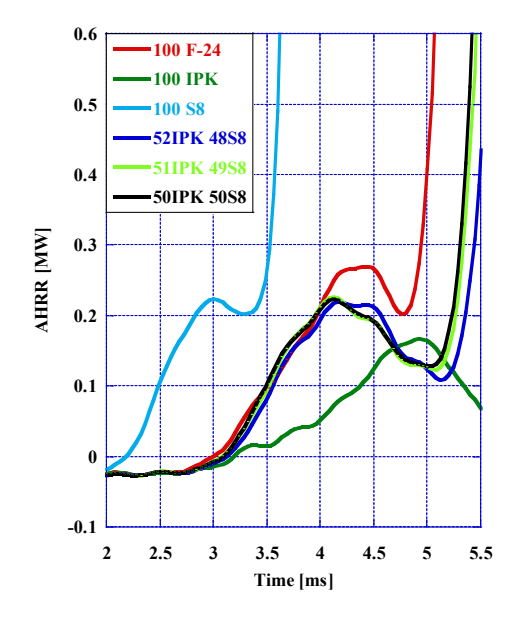


Figure 14. LTHR of Surrogate Fuels

The LTHR region of F-24 could not be reproduced by any of the surrogate fuels due to the longer ID of neat IPK which extended the NTC regions for the surrogates.

The LTHR durations and percent difference compared to F-24 for all the researched fuels are shown in Table 9. The surrogate 50IPK 50S8 was found to have the smallest percent difference compared to F-24 at 9.90%.

Table 9. LTHR Durations of Researched Fuels

Researched	LTHR	% Difference
Fuels	Duration [ms]	
100 F-24	1.92	-
100 IPK	9.56	133.10
75IPK 25S8	3.40	55.64
52IPK 48S8	2.24	15.38
51IPK 49S8	2.20	13.59
50IPK 50S8	2.12	9.90
25IPK 75S8	1.56	20.69
100 S8	1.26	41.51

The energy released during the LTHR region and percent difference compared to that of F-24 of the researched fuels can be seen in Table 10. The blend 52IPK 48S8 was determined to have the lowest percent difference of 1.54% when compared to F-24.

Table 10. LTHR Energy Release for Researched Fuels

Table 10. LTTIK Energy Release for Researched Fuels					
Researched	LTHR Energy	% Difference			
Fuels	Release [J]				
100 F-24	336.61	-			
100 IPK	476.81	34.47			
75IPK 25S8	374.17	10.57			
52IPK 48S8	331.47	1.54			
51IPK 49S8	330.72	1.77			
50IPK 50S8	328.15	2.55			
25IPK 75S8	262.10	24.89			
100 S8	206.23	48.04			

The peak combustion temperatures for the researched fuels can be found in Table 11. Temperature is derived from the Ideal Gas Law, as shown in Equation 5 where V is the volume of the CVCC, P is pressure, R is the gas constant of ambient air, n is the number of moles of the fuel, and T is the absolute temperature.

$$T = \frac{PV}{nR}$$
 Eq. 5

The peak temperature of the fuels was observed to decrease with the addition of S8.

Table 11. Peak Temperature for Researched Fuels

Researched Fuels	Peak Temperature [K]
100 F-24	1846.7
100 IPK	1852.8
75IPK 25S8	1847.6
52IPK 48S8	1829.9
51IPK 49S8	1829.8
50IPK 50S8	1828.0
25IPK 75S8	1828.6
100 S8	1813.9

Mass Fraction Burned

The percent mass fraction burned for the researched fuels can be seen in Figure 15. Fuels with a higher DCN correlate to a better auto-ignition quality which is observed by an increased rate of combustion and mass fraction burned. Neat S8 was observed to combust faster than all the other fuels, burning all its mass 4.56ms after the start of injection, while neat IPK had the longest combustion, burning all its mass after 20.64ms.

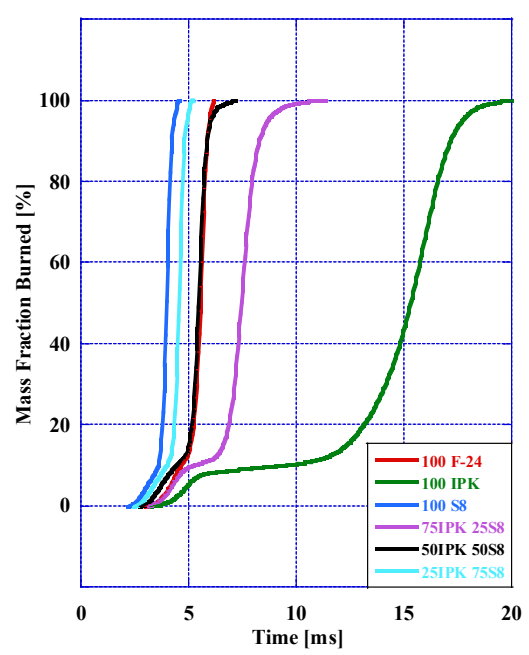


Figure 15. Mass Fraction Burned of the Researched Fuels

Noise Vibration and Harshness (NVH) Analysis

Through the application of a Hottinger Brüel and Kjær accelerometer, seen in Figure 16, the combustion processes of 100% F-24, S8 and IPK were evaluated with respect to the AHRR of each fuel. Vibrations from the combustion of F-24, S8 and IPK were measured and the combustion phasing was listed on the graph, shown in Figures 17-19.

The acceleration produced by each fuel's combustion in m/s^2 is on the Y-axis of the plot with respect to time in milliseconds (ms) presented on the X-axis. Through the

processing of acceleration with respect to time in ms, the combustion vibrations produced by each fuel were correlated to each fuel's respective AHRR.

The durations of Ignition Delay (ID) and Combustion Delay (CD), as seen in Table 6, were applied over the combustion vibrations produced by each fuel, shown in Figures 17-19.

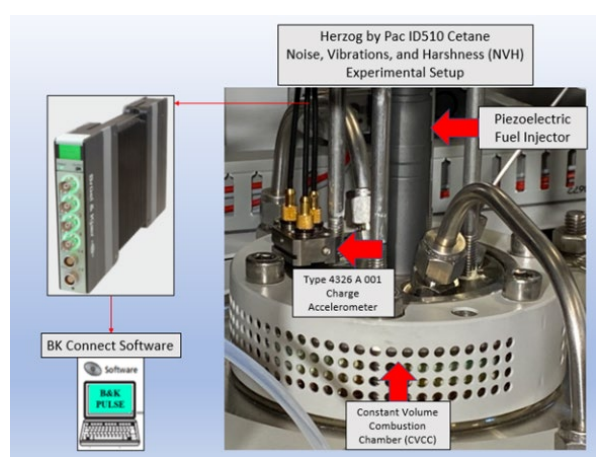


Figure 16. NVH Instrumentation on CVCC

From the assessment of the combustion vibrations produced by F-24, S8 and IPK it was verified that the greatest duration of ID and CD occurred within the combustion of IPK. Specifically, the ID of IPK was 18.47% longer than F-24 and 15.21% longer than S8. The difference seen in the CD of IPK compared to F-24 and S8 was far greater. Neat IPK was 176.39% longer in duration than F-24 and 282.42% longer in duration than S8. These values correlate between the Figures 17-19 and Table 6.

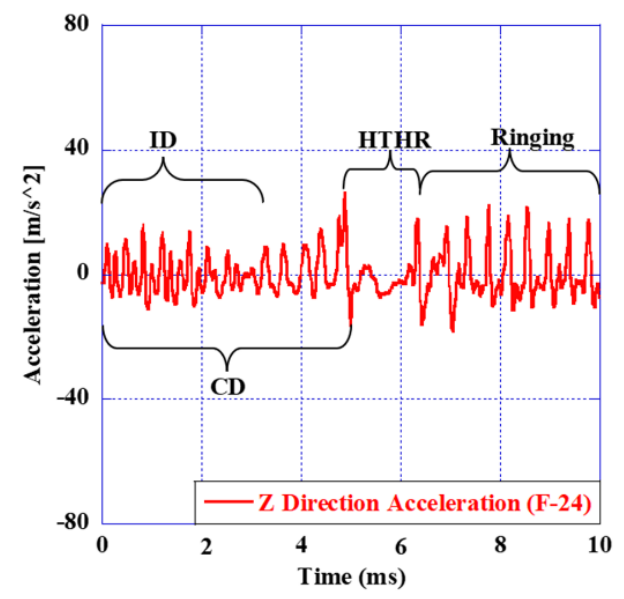


Figure 17. Z Direction Combustion Acceleration with Relation to AHRR of neat F-24

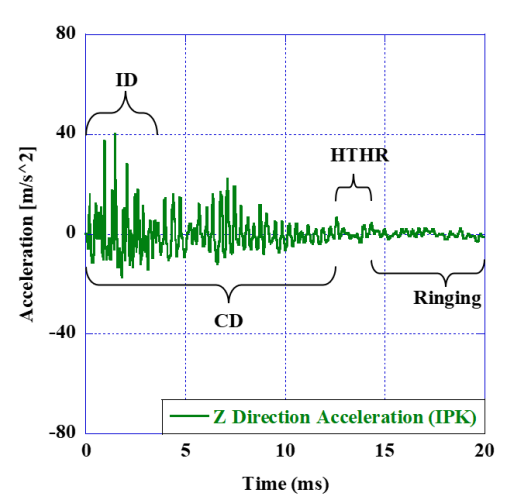


Figure 18. Z Direction Combustion Acceleration with Relation to AHRR of neat IPK

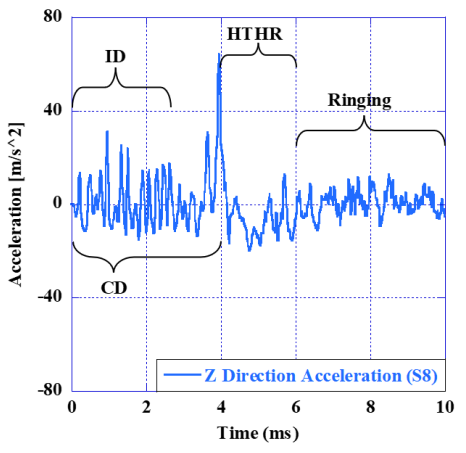


Figure 19. Z Direction Combustion Acceleration with Relation to AHRR of neat S8

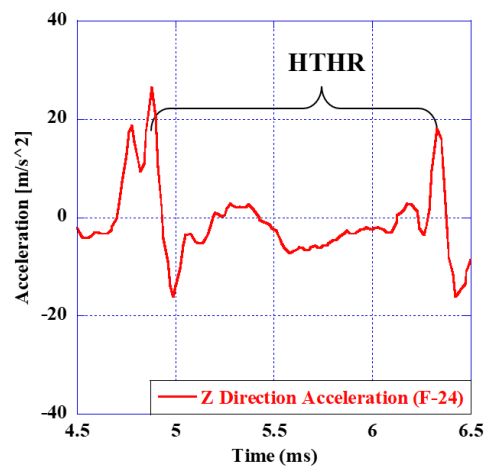


Figure 20. Vibrations Pattern during HTHR of F-24

More importantly, the vibrations during the HTHR region in each of the Figures 17-19 have a repeating trend that is the same across all the researched fuels, this can be seen in detail in Figure 20. In general, the vibrations produced during HTHR have the lowest values.

Conclusion

Research was conducted in a CVCC to investigate the autoignition quality and combustion properties of blends of two Sustainable Aviation Fuels (SAF), IPK and S8 to determine a surrogate fuel for F-24. The thermophysical properties of the neat fuels were also determined to gain a wider perspective on their combustion characteristics. Neat IPK was found to have a higher Lower Heating Value.

A spray analysis was conducted using a He-Ne laser utilizing Mie scattering theory and Fraunhofer assumptions. It was observed that neat IPK had the smallest SMD and distribution for 10%, 50% and 90% of the spray and was observed to have the most favorable thermal-physical properties of the neat fuels; however, the large CD significantly reduced the DCN of IPK.

The pressure curves during combustion of 52IPK 48S8, 51IPK 49S8 and 50IPK 50S8 were observed to closely overlap with that of neat F-24. The influence of IPK in the blends was observed to decrease peak pressure ringing and correspond to greater combustion stability.

During the peak of the AHRR curve, 50IPK 50S8 had the closest matching max values to F-24, while 51IPK 49S8 was observed to more closely follow the AHRR trend of F-24.

The LTHR analysis of F-24 could not be reproduced using the surrogate fuels, as the influence of IPK in the blend was seen to extend the NTC region due to its greater ID and CD values. This is in contrast to that of the other fuels. The surrogate blend 50IPK 50S8 was observed to have the lowest percent difference during the duration of LTHR when compared to F-24 and 52IPK 48S8 was found to have the lowest percent difference in energy release during LTHR compared to F-24. It was learned that the influence of S8 in the fuels decreased the duration of the LTHR and the presence of IPK in the blend increases the NTC region. The cool flame region for F-24 is longer in duration than that of S8, while the NTC region is slightly shorter. Additionally, the cool flame formation of F-24 was observed to have periods of ignition and quenching of about 0.5ms. The 25% blends were very far from the F-24 target in terms of combustion properties.

During the NVH analysis of the combustion of the neat fuels in the CVCC it was found that the ID, CD and HTHR have an influence on vibrations occurring during combustion and subsequent ringing. Vibrations occurring during HTHR had a recurring pattern across the neat fuels. Additionally, the vibrations were observed to be lower during HTHR. From the NVH analysis it can be observed that neat S8 had the most violent start of combustion of the three neat fuels, resulting in the highest acceleration values in the combustion chamber.

Acknowledgments

Acknowledgement of the Air Force Research Laboratory for supplying experimental fuels. We would also like to acknowledge Charles McGuffy, Michael Rankin and Jacques Lapeyre from PAC concerning the PAC CID 510, Joseph Wolfgang from Malvern Lasers and Tanner Smith, Tony Frazer, Ryan Salmon, and Alfonso Moreira from Hottinger Brüel and Kjær. This paper is based upon work supported by the National Science Foundation Grant No. 1950207.

References

- [1] J. Guzman and K. Brezinsky, "Experimental and Modeling Study of the Oxidation of F-24 jet fuel, and its Mixture with an Iso-paraffinic Synthetic jet fuel, ATJ," Combustion and Flame, vol. 224, pp. 108–125, 2021.
- [2] V. Soloiu, R. Gaubert, J. Moncada, J. Wiley, J. Williams, S. Harp, M. Ilie, G. Molina, and D. Mothershed, "Reactivity Controlled Compression Ignition and Low Temperature Combustion of Fischer-Tropsch Fuel Blended with N-Butanol," Renewable Energy, vol. 134, pp. 1173–1189, 2019. https://doi.org/10.1016/j.renene.2018.09.047
- [3] C. Atkinson, G. Thompson, M. Traver, and N. Clark, "In-Cylinder Combustion Pressure Characteristics of Fischer-Tropsch and Conventional Diesel Fuels in a Heavy Duty CI Engine," SAE Transactions, vol. 108, pp. 813–836, 1999.
- [4] Y. Jiao, R. Liu, Z. Zhang, C. Yang, G. Zhou, S. Dong, and W. Liu, "Comparison of Combustion and Emission Characteristics of a Diesel Engine Fueled with Diesel and Methanol-Fischer-Tropsch Diesel-Biodiesel-Diesel Blends at Various Altitudes," Fuel, vol. 243, pp. 52–59, 2019.
- [5] S. Jürgens, P. Oßwald, M. Selinsek, P. Piermartini, J. Schwab, P. Pfeifer, U. Bauder, S. Ruoff, B. Rauch, and M. Köhler, "Assessment of Combustion Properties of Non-Hydroprocessed Fischer-Tropsch Fuels for Aviation," Fuel Processing Technology, vol. 193, pp. 232–243, 2019.
- [6] S. S. Gill, A. Tsolakis, K. D. Dearn, and J. Rodríguez-Fernández, "Combustion Characteristics and Emissions of Fischer–Tropsch Diesel Fuels in IC Engines," Progress in Energy and Combustion Science, vol. 37, no. 4, pp. 503–523, 2011.
- [7] H. Wang and M. A. Oehlschlaeger, "Autoignition Studies of Conventional and Fischer–Tropsch Jet Fuels," Fuel, vol. 98, pp. 249–258, 2012.
- [8] V. Soloiu, C. J. Phillips, C. Carapia, A. Knowles, D. Grall, and R. Smith, "Exploratory Investigation of Combustion and NVH Signature of a Drone Jet Engine Fueled with IPK," AIAA Scitech 2021 Forum, 2021. https://doi.org/10.2514/6.2021-1347

- [9] S. I. Mussatto, I. L. Motta, R. M. Filho, L. van der Wielen, R. Capaz, J. Seabra, P. Osseweijer, J. Posada, M. de Freitas Gonçalves, P. R. Scorza, and G. Dragone, "Sustainable Aviation fuels: Production, Use and Impact on Decarbonization," *Comprehensive Renewable Energy*, pp. 348–371, 2022.
- [10] P. Kurzawska, "Overview of Sustainable Aviation Fuels Including Emission of Particulate Matter and Harmful Gaseous Exhaust Gas Compounds," Transportation Research Procedia, vol. 59, pp. 38–45, 2021.
- [11] C. Jiang and H. Yang, "Carbon tax or Sustainable Aviation Fuel Quota," Energy Economics, vol. 103, p. 105570, 2021.
- [12] P. M. Smith, M. J. Gaffney, W. Shi, S. Hoard, I. I. Armendariz, and D. W. Mueller, "Drivers and Barriers to the Adoption and Diffusion of Sustainable Jet Fuel (SJF) in the U.S. Pacific Northwest," Journal of Air Transport Management, vol. 58, pp. 113–124, 2017.
- [13] D. Selvatico, A. Lanzini, M. Santarelli, "Low Temperature Fischer-Tropsch Fuels from Syngas: Kinetic Modeling and Process Simulation of Different Plant Configurations," Fuel, vol. 186, pp. 544-560, 2016.
- [14] P. M. Maitlis and A. de Klerk, Greener Fischer-Tropsch Processes: for Fuels and Feedstocks. John Wiley & Sons, 2013.
- [15] N. H. Leibbrandt, A. O. Aboyade, J. H. Knoetze, and J. F. Görgens, "Process Efficiency of Biofuel Production via Gasification and Fischer–Tropsch Synthesis," Fuel, vol. 109, pp. 484–492, 2013.
- [16] R. G. D. Santos and A. C. Alencar, "Biomass-Derived Syngas Production via Gasification Process and its Catalytic Conversion into Fuels by Fischer Tropsch Synthesis: A review," International Journal of Hydrogen Energy, 2019.
- [17] V. B. Borugadda, G. Kamath, and A. K. Dalai, "Technoeconomic and Life-cycle Assessment of Integrated Fischer-Tropsch Process in Ethanol Industry for Bio-Diesel and Bio-Gasoline Production," Energy, vol. 195, p. 116985, 2020.
- [18] T. Damartzis and A. Zabaniotou, "Thermochemical Conversion of Biomass to Second Generation Biofuels through Integrated Process Design—A Review," Renewable and Sust. Energy Reviews, vol. 15, no. 1, pp. 366–378, 2011.
- [19] V. Soloiu, J. T. Wiley, R. Gaubert, D. Mothershed, C. Carapia, R. C. Smith, J. Williams, M. Ilie, and M. Rahman, "Fischer-Tropsch Coal-to-Liquid Fuel Negative Temperature Coefficient Region (NTC) and Low-Temperature Heat Release (LTHR) in a Constant Volume Combustion Chamber (CVCC),"

- Energy, vol. 198, p. 117288, 2020. https://doi.org/10.1016/j.energy.2020.117288
- [20] V. Soloiu, R. Smith, A. Weaver, D. Grall, C. Carapia, L. Parker, M. Ilie, M. Rahman, and G. Molina, "Investigations of Low-Temperature Heat Release and Negative Temperature Coefficient Regions of Iso-Paraffinic Kerosene in a Constant Volume Combustion Chamber," ASME 2021 Internal Combustion Engine Division Fall Technical Conference, 2021. https://doi.org/10.1115/ICEF2021-68203
- [21] A. F. Alhikami and W. Wang, "Experimental Study of the Spray Ignition Characteristics of Hydro-Processed Renewable Jet and Petroleum Jet Fuels in a Constant Volume Combustion Chamber," Fuel, vol. 283, 2021.
- [22] F. K. Tsuji and L. D. Neto, "Influence of Vegetable Oil in the Viscosity of Biodiesel A Review," SAE Technical Paper Series, 2008. doi:10.4271/2008-36-0170.
- [23] K. Wan, J. Manin, H. S. Sim, and I. Karathanassis, "Soot and PAH Formation in High Pressure Spray Pyrolysis of Gasoline and Diesel Fuels," Combustion and Flame, vol. 241, p. 112084, 2022.
- [24] K. C. Kalvakala, P. Pal, J. P. Gonzalez, C. P. Kolodziej, G. Kukkadapu, S. Wagnon, R. Whitesides, N. Hansen, and S. K. Aggarwal, "Numerical Analysis of Soot Emissions from Gasoline-Ethanol and Gasoline-Butanol 1 Blends under Gasoline Compression Ignition Conditions," SSRN Electronic Journal, 2022.
- [25] Soloiu, V., Weaver, A., Parker, L., Brant, A., Smith, R., Ilie, M., Molina, G., & Damp; Carapia, C. (2022). Constant Volume Combustion Chamber (CVCC) Investigations of Aerospace F-24 and Jet-A in Low-Temperature Heat Release and Negative Temperature Coefficient Regions. Energy Conversion and Management, 263, 115687. https://doi.org/10.1016/j.enconman.2022.115687
- [26] Heywood, J. 1988, Internal Combustion Engine Fundamentals, McGraw-Hill, New York.
- [27] Y. Ju, C. B. Reuter, O. R. Yehia, T. I. Farouk, and S. H. Won, "Dynamics of Cool Flames," Progress in Energy and Combustion Science, vol. 75, p. 100787, 2019.